SPECTRAL AND STRUCTURAL ANALYSIS FOR SODIUM SILICATE-BASED AEROGEL VIA NORMAL DRYING PRESSURE

Wasan H. Al-husseny[1a], Israa F. Al-sharuee[2a] and Ban R. Ali[3a]

Abstract: Five types of silica aerogel were prepared at ambient pressure: sodium silicate, TEOS, and sodium silicate, with TEOS utilized as precursors. We investigated the effects of catalysis, mixing water or ethanol with the precursors, as well as the procedure of modification. Aqueous is a low-cost alternative, and many applications utilize it. A manufacturing colloidal silicic acid hydrosol was created from the ion exchange of an industrial water glass. The properties of physical, chemical, and hydrophobicity were examined via density, XRD, FTIR, and contact angle. BET, FESEM, and EDS analysis determined the structural properties. The silica hydrogel's pore liquid (H_2O) was successively removed. The spectral properties confirmed the modification by the derived high contact angle of 152º, low transparency, and amorphous structure. The resulting aerogel monoliths have a well-developed mesoporous structure, a large specific surface area of 961 m2/g, and a low density of 0.04 g/cm3.

Keywords: Ambient pressure, sodium silicate, aerogel, hydrophobicity, contact angle

1. Introduction

Silica aerogel has a three-dimensional nanoporous structure. An aerogel is an ultra-porous substance with a strongly cross-linked network structure, 90% composed of pores (Dorcheh & Abbasi, 2008). These are made up of mesopore cells, which are semitransparent and heat-insulating materials (Huang et al., 2019). It has several unique features, including a good specific surface area and good porosity (Feng et al., 2018; He & Chen, 2017; Pan et al., 2017), optical transmission (99%), high porosity (98%), and low thermal conductivity (0.01 W/mK) (Al-Mothafer, Abdulmajeed, & Al-Sharuee, 2021). They have attracted great interest and demonstrated good market potential. This has the potential to be employed in a variety of fields, including adsorption (Israa F Al-sharuee & Mohammed, 2019; Mazrouei-Sebdani, Salimian, Khoddami, & Shams-Ghahfarokhi, 2019; Wingfield, Franzel, Bertino, & Leventis, 2011), thermal insulation (Israa F Al-sharuee, 2019; X.-D. Wang, Sun, Duan, & Hu, 2013), sensors and dielectrics (He et al., 2019), fusion targets (Daniel, Longo, Ricciardi, Reverchon, & Guerra, 2013; Wagh, Ingale, & Gupta, 2011), and catalysts (Zhang, Chen, Zhang, Ye, & Cui, 2021). The sol-gel technique was employed to produce silica, which comprised the reaction of water with the silica precursor in the presence of a solvent such as acetone or ethanol, as well as the use of a necessary catalyst and supercritical drying during the final stage (Aegerter, Leventis, & Koebel, 2011).

Two types of silicon precursors are used to make silica aerogels. Organ silanes can be tetraethoxysilane TMOS, methyl-hydro siloxane PMHS (Bhagat & Rao, 2006; Nguyen et al., 2010) or Na_2SiO_3 (Al-Mothafer & Abdulmajeed, 2021). TEOS may produce wet gels, although it has fractures and can break into small pieces under normal pressure. Wet gels composed from xerogels use a vapor passing technique or ion exchange procedures to make the water glass-based aerogels, which include eliminating the sodium from the water glass (Durães et al., 2012). Several studies have found that hexadecyltrimethoxysilane with tetraethoxysilane or dimethyl diethoxy silane with tetraethoxysilane was employed to make hydrophobic silica aerogels (Zhou, Shen, Wu, Wu, & Ni, 2007). Silica sol and tetraethoxysilane are examples of organic-inorganic materials (Li, Jiang, Xu, Hai, & Zheng, 2016). Researchers have paid close attention to cost-effective and efficient preparation methods for silica aerogel powders. In two hours, Wang et al. (2015) were able to obtain silica aerogel powders. However, they employed tetraethyl orthosilicate as a precursor, which is expensive and difficult to apply in large-scale industrial manufacturing (J. Wang, Zhang, Wei, & Zhang, 2015). Yajun Huang et al. (2012) investigated the production of water glass-based aerogel granules. Under ambient pressure drying, organic solvents can be saved. Within six hours, a unique method of preparing nano porous silica aerogel was reported under ambient pressure. The resulting silica aerogel has a homogeneous

Authors information:
[a]Department of Physics, College of Science, Mustansiriyah University, Baghdad, IRAQ. E-mail: wasanhassan@uomustansiriyah.edu.iq[1]; i81f54@uomustansiriyah.edu.iq[2;] banrasheed2003@yahoo.com[3]
*Corresponding Author: i81f54@uomustansiriyah.edu.iq

mesoporous structure and low thermal conductivity (0.0237–0.0245 W/mK at 1 atm), according to the results of the tests (Monshi, Foroughi, & Monshi). In this work, five types of silica aerogel were prepared at ambient pressure: sodium silicate, TEOS, and sodium silicate, with TEOS utilized as precursors. The effects of the catalysis, mixing water or ethanol with the precursors, and the procedure of modification, were investigated.

2.   Experimental Part

2.1 Materials

Sodium silicate powder (Na_2SiO_3), M.W.212.14 g/mol, 99.9%), and Tetraethylorthosilicate Si $(OC_2H5)_4$ (TEOS, 98%) were obtained from Sigma-Aldrich, (Germany). Trimethylchlorosilane $(CH_3)_3SiCl$ (TMCS > 98%) (TCI Japan) and n-Hexane (C_6H_{14} > 98 %) were obtained from Chemo-LAB (Belgium). Ethanol was obtained from Schariau (Spain) (99%). CDH provided hydrochloric acid (MW 36.45g/mol, 99.0%) and ammonium solution (NH_4OH M.W. 17.03 g/mol) (INDIA). Amberlite (IR-120 Na)

2.2 Sample preparation and characterization methods

Five samples were prepared for the production of hydrophobic silica aerogel. The flow chart illustrates the preparation steps undertaken. The completion of modification and the band vibration were prepared by FTIR spectroscopy (Bruker FTIR Spectrometer ALPHA II, USA). The crystallites were validated using XRD analysis (GaliPIX3D X-ray Detector | 2D Hybrid Pixel XRD Detector) (1.5406 A°). The green size was calculated by the Scherrer Equation (Monshi et al., 2012):

$$L = \frac{K\lambda}{\beta \cos\theta} \qquad (1)$$

where K is constant, and is most commonly taken as 0.9, λ is the wavelength of the X-ray at 1.5406 A° at full width and at half maximum of peak, and θ is the Braggs angle. The morphology and percentage of the elements involved FESEM and EDS analysis. Mass and volume measurements were used to calculate the bulk density of the aerogel. The volume was calculated using V= R^2h, where R is the radius and h is the height. The bulk density = m/V if "m" signifies its mass. Besides the specific surface area and average pour volume, they were determined via BET analysis (BELSORP-mini II) at varied partial pressures ($0.01p/p_{01}$). Contact angle measurements were used to evaluate the hydrophobicity (3μ). The volume of a water drop was placed on the top surface of a sample. The contact angle (θ) was determined using the equation (2), where h, w is the drop's height and width, respectively (Khedkar, Somvanshi, Humbe, & Jadhav, 2019; Zhao, Li, & Zhang, 2018).

$$\theta = 2\tan^{-1}\frac{2h}{w} \qquad (2)$$

Five different types of samples were produced: W1, W2, W3, W4, and W5. W1 and W2 are similar in preparation but differ in the washing process: after being converted to gel, W1 was soaked in (50% water+50% ethanol) for 24 hours twice, whereas W2 was soaked in (100% ethanol) for 24 hours twice. W3 was prepared from condensed silica only with (TEOS: Eth: HCl [0.1M]) with (2.17: 5: 0.23). W4 is similar to sample W1, but differs by not adding HCl before ion exchange. W5 was prepared from silicic acid only (the ratio of sodium silicate to distilled water was 1:4). All samples were converted to gel by adding 1N of NH4OH drop by drop, and the surface modification by TMCS and n-Hexane were preserved at a ratio of [1:6 M] at 60 °C for 24 hours. Then n-Hexane was added for 24 hrs, two times around the holder in a small perforated plastic lid before allowing it to dry at ambient pressure for 72 hrs. The samples were then placed under 120 °C every 10 °C to obtain the hydrophobic silica aerogel.

3. Results and Discussion

3.1. FTIR analysis

Tables 1 and 2 and Figure 1 illustrate the hydrophobicity properties and vibrational alterations as a result of FTIR spectra, where υ, stretching vibration; $υ_s$, symmetric stretching vibration; $υ_{as}$, antisymmetric stretching vibration; δ, deformation vibration; $δ_s$, symmetric deformation vibration (bending); and $v_β$, in-plane stretching vibration (Shirtcliffe, McHale, Newton, & Perry, 2003). From FT-IR, Si-CH₃ at 3995 cm^{-1} indicates that a considerable fraction of the Si atoms on the surface was hydroxylated. The O-H stretching band of hydrogen 3995 cm^{-1} linked water molecules caused the broad absorption peak centered at cm^{-1} (H-O-H). Peaks at 2057 cm^{-1} and 1480 cm^{-1} correspond to OH and Si-OH, respectively, indicating that the silica surface remains unchanged (Bhagat et al., 2008; Cheng et al., 2016). Peaks at 842 cm^{-1} and 2995 cm^{-1} are attributed to Si-CH₃ bending at 1200 cm^{-1}. These peaks are the result of TMCS altering the surface of the silica aerogel. The hydrophilic (Si-OH) types were replaced by hydrophobic (Si-CH₃) collections when the gel surface was changed with Hexane-TMCS solution, as evidenced by the disappearance of a peak at 1131 cm^{-1}. The irregular stretching and bending vibrations, which correspond to Si-O-Si bonding, demonstrate a significant absorption peak at 1055 cm^{-1} and 1045 cm^{-1}, respectively (Sarawade, Kim, Hilonga, & Kim, 2010; Shi et al., 2017).

Table 1. The vibration of bands as a result of FTIR examination

Type of vibration Sample	Si-OH H-OH	υsC-H	υ_{as}C-H	δH-O-H	δ_sSi-CH	υ_{as}Si-O-Si	υ_βSi-OH	vSi-CH	v_sSi-O-Si
W1	3650	2971	2177	1706	1262	1065	1138	842	488
W2	3745	2963	2366	2054	1250	1043	1177	841	450
W3	3746	2986	2346	1774	1266	1067	1126	844	468
W4	3753	2963	2362	2089	1255	1072	1137	841	442
W5	3760	2362	2961	1699	1257	1060	1130	845	439

Table 2. Percentage of intensity variation depended on Si-O-Si length

sample	length	Si-OH	Si-CH	CH	OH
W1	81.70	1.317	4.47	17.58	35.55
W2	94.07	2.64	3.12	15.73	35.79
W3	80.43	2.76	3.14	15.49	35.78
W4	79.82	1.93	2.65	14.55	37.15
W5	78.69	15.23	28.65	14.14	35.78
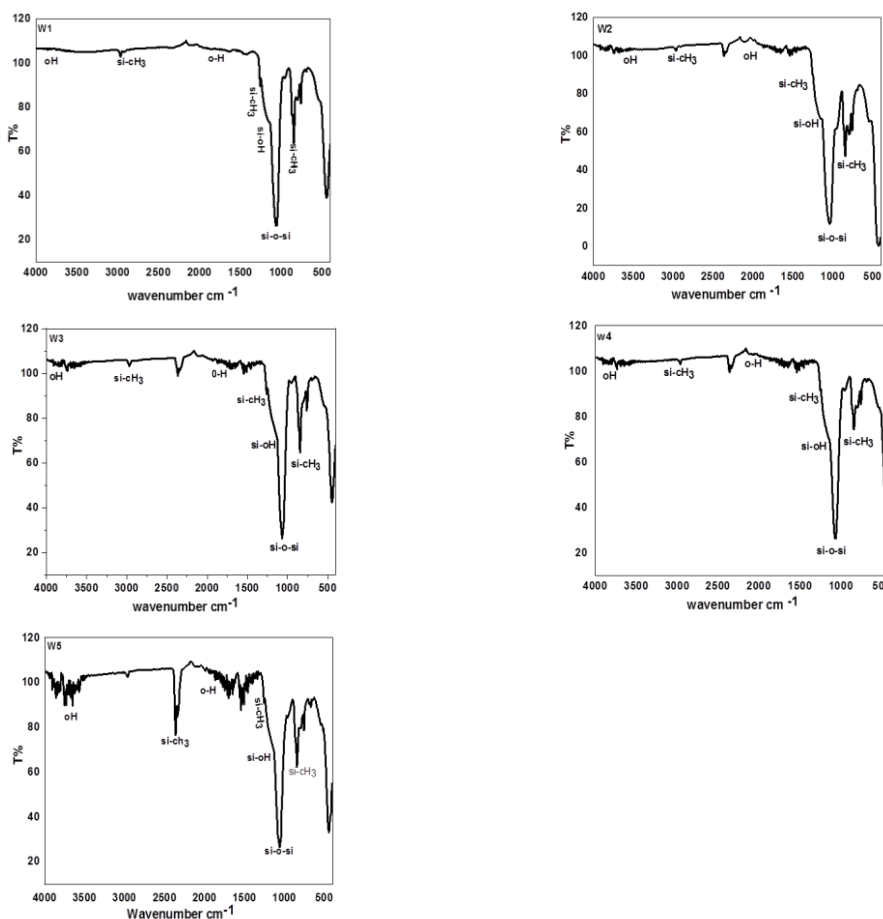
Figure 1. FTIR spectrum for W1, W2, W3, W4 and W5 samples

3.2. Contact angle measurements

The contact angle between a water drop supported on an external surface and the surface under investigation can be used to measure hydrophobicity (Khedkar et al., 2019). Figure 2 (a, b, c, d, and e) demonstrates the effect of environmental preparation on the contact angle and the variation in the contact angle of the aerogel samples for W1, W2, W3, W4, and W5. When adding HCl to resin W1 and W2, the contact angle increased, while the gel time took three times longer; this may help to complete the modification, resulting in a contact angle of 150.89° and a surface area of 961.1m²/g. The contact angle for W2 was 147.89° and the surface area was 674.88m²/g, as shown in Table 3. More

transparency and a surface area of 790.49 m²/g and a short gel time were found in the W3; because that particular sample was only TEOS. In terms of W4; without adding HCl to the resin, the contact angle was decreased. More overcast, small surface area, and lowest gel time were found in the W5 sample, as well as a light weight, despite a density of 0.04 g/cm³ and a high contact angle of 152˚. The reason is that sample was only sodium silicate containing sodium salts after it began to replace the hydroxide group attached to silicon with a chloride group, leading to a good modification process.
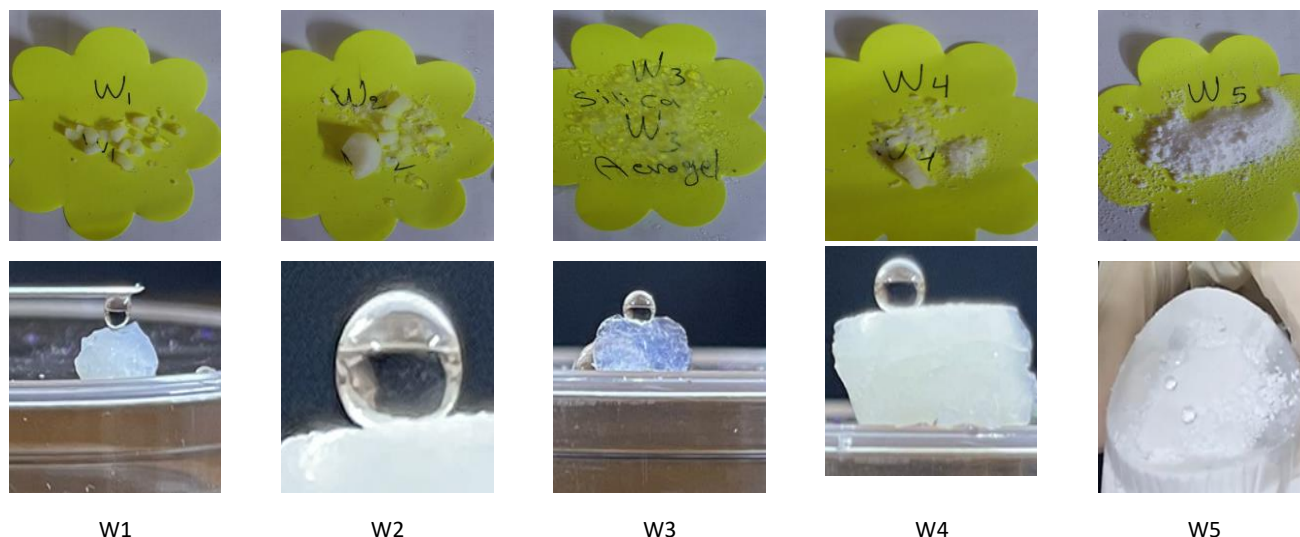
Figure 2. The photographs of superhydrophobic aerogels for W1,W2 , W3, W4 and W5 samples

Table 3. Some of physical properties for silica aerogel prepared in different methods

Sample	Vm (cm³/g)	Surface aera (m²/g)	Total pore volume (cm³/g)	Mean pore diameter (nm)	Average Particle size	Gel time min	Density g/cm³	Contact angle
W1	158.78	961.1	2.23	12.941	38.618	120	0.156	150.89°
W2	155.06	674.88	2.2404	13.279	42.758	120	0.296	147.89°
W3	181.62	790.49	2.8498	14.42	43.23	15	0.096	138.70°
W4	159.1	692.47	1.67	9.6634	39.49	30	0.135	141.68°
W5	25.172	109.56	0.2962	10.815	53.648	10	0.04	152°

3.3. XRD analysis

Figure 3 depicts the X-Ray Ddiffraction of the samples (W1, W2, W3, W4, and W5). The size granule estimates for each sample are shown in Table 4. The difference between W1W2 and W4 is the addition of HCl to sodium silicate before it makes the ionic exchange and the difference between W1 and W2 in the way of washing. This means that the stimulation of cation resin plays an important role in making an amorphous sample similar to the silica aerogel from TEOS parcourse, as shown in samples W2 and W4, which indicate an amorphous structure with a broad band at 2θ between 22-34 degrees, and for W4 at 2θ between 18-28 degrees.
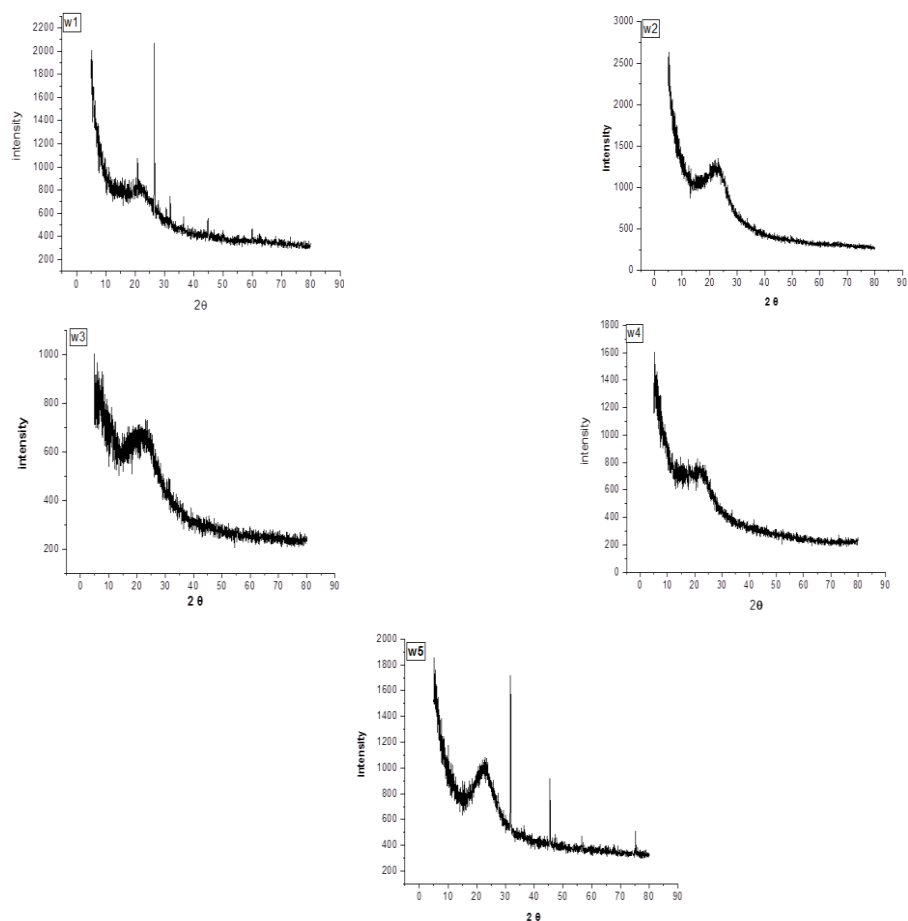
Figure 3. XRD diagram for W1, W2, W3, W4 and W5 silica aerogel prepared in different methods

Table 4. FWHM and grain size for W1, W2, W3, W4 and W5 silica aerogel

	2θ	Height	FWHM	Grain size
	20.82	196	0.06	23.49
	26.599	1195	0.11	12.95
	30.56	100	0.08	17.97
	31.97	221	0.08	18.08
	36.54	106	0.06	24.35
W1	39.50	40	0.1	14.72
	40.2	29	0.1	14.87
	42.5	29	0.2	7.435
	44.86	166	0.08	18.75
	45.95	46	0.1	15.06
	50.1	31	0.3	5.104
	59.96	99	0.11	14,55
	0.1767	8	111	229
W3	0.1769	8	56	23.0
	23	40	3	0.47
	27.32	56	0.05	28.87
	31.70	944	0.089	16.07
W5	45.48	471	0.143	10.51
	56.49	104	0.10	15.75
	75.27	171	0.09	19.46

3.4. BET analysis

Figure 4 depicts the linear N2 adsorption-desorption isotherm plots for aerogel samples prepared using various approaches. In most mesoporous to microporous materials, a hysteresis loop is present, which is linked to capillary condensation and evaporation in the mesopores. It was observed that the W1 and W2 samples have well-defined cylindrical pore channels of the H1 type. The surface area of silica aerogel appears to be enormous at 961.1 m^2/g based on the BET measurement of sample W1. It is likely that the observation is attributable to the sample's pore volume of 2.359 cm^3/g. W2 is 674.88 m^2/g because of the pore volume of 2.240 cm^3/g of the pores found in the taster (Israa F AL-Sharuee,

2021). Meanwhile, it seems that samples W3 and W4 may be categorized as H2 type disordered pores (pore blocking) percolation phenomena, which are related to the surface part of the silica aerogel. This appears that based on the BET analysis of sample W3. Sample W5 has a pore volume of 2.848 cm^3/g and a surface area of 790.4 m^2/g, and belongs to the H3 category, which consists of non-rigid aggregates of plate-like particles (slit-shaped pores). The silica aerogel looks to have a small surface area, since it is merely sodium silicate at 109.56 m^2/g. It is not as dense as other samples. It is possible that the observation is the result of increased pore volume and density (Pan et al., 2017; Shao, Luo, Cheng, & Zhang, 2013).

W1

W2

W3

W4

W5
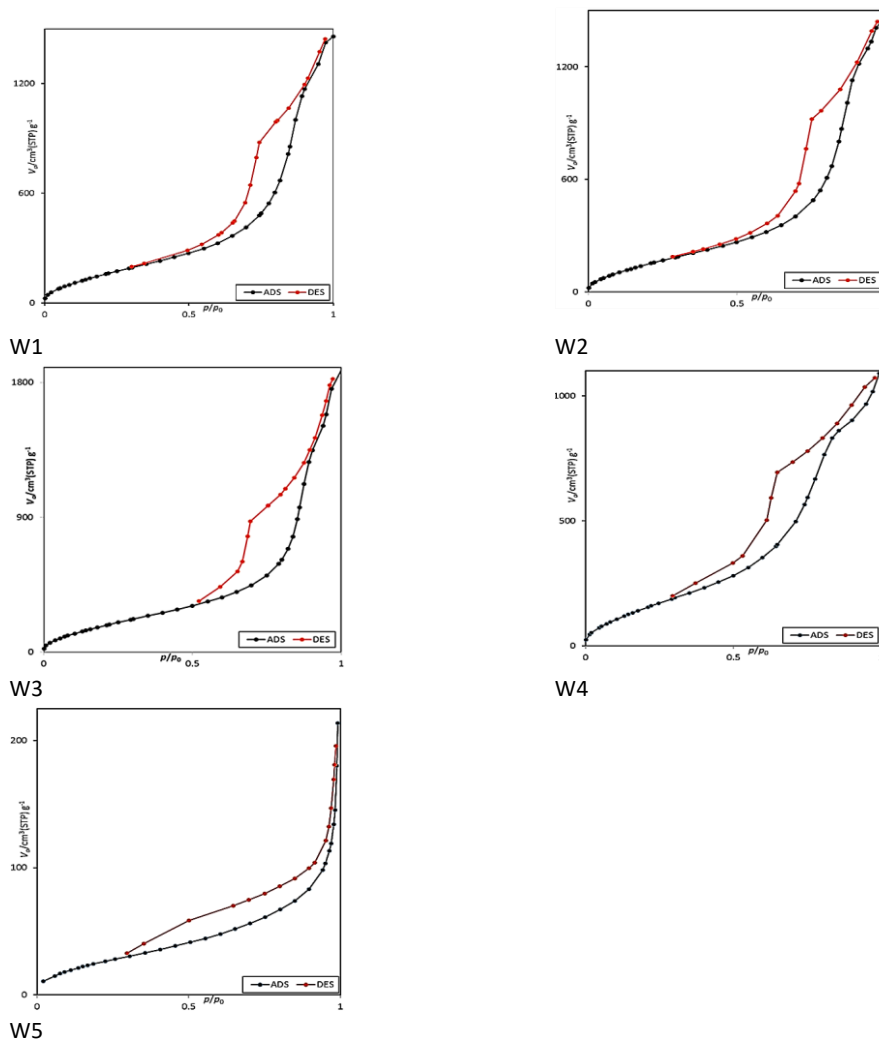
Figure 4. N2 adsorption–desorption isotherms for W1, W2,W3,W4 and W5 samples

3.5. FE-Scanning Electron Microscopy and EDS images

Figure 5 depicts the FE-SEM and EDS images for the W1, W2, W3, W4 and W5 samples. In 200 nm of FE-SEM, the microstructure of sample W1 contains a continuous and extensively cross-linked network, resulting in an extremely open structure with individual particles that cannot be separated and an average particle size of 38.618 nm. The microstructure of W2 indicates that the particles are aggregations with a smooth surface form. The silica aerogel features a three-dimensional network and a small ball shape. Furthermore, microstructural

homogeneity was observed, with the average particle count in sample W3 being 42.758nm. The microstructure of sample W3 appeared to be clusters of silica aerogel, and the particles were packed together with a smooth surface. There was also microstructural inhomogeneity, with the average particle size of the sample being 34.23 nm. At W4, the silica aerogel's fracture structure comprises highly branched clusters of smaller particles. The large pores can be seen rising from the fracture surface; there are no aggregations, and the surface is rough. In addition, the sample had no microstructural homogeneity, and the average

particle count was 38.618 nm. Finally, the silica aerogel in sample W5 resembles tree blooms; the particles are also aggregations, and the surface was smooth. Furthermore, the sample had microstructural inhomogeneity because of sodium silicate, which is a minor part of its structure, with an average particle count of 53.648 nm.
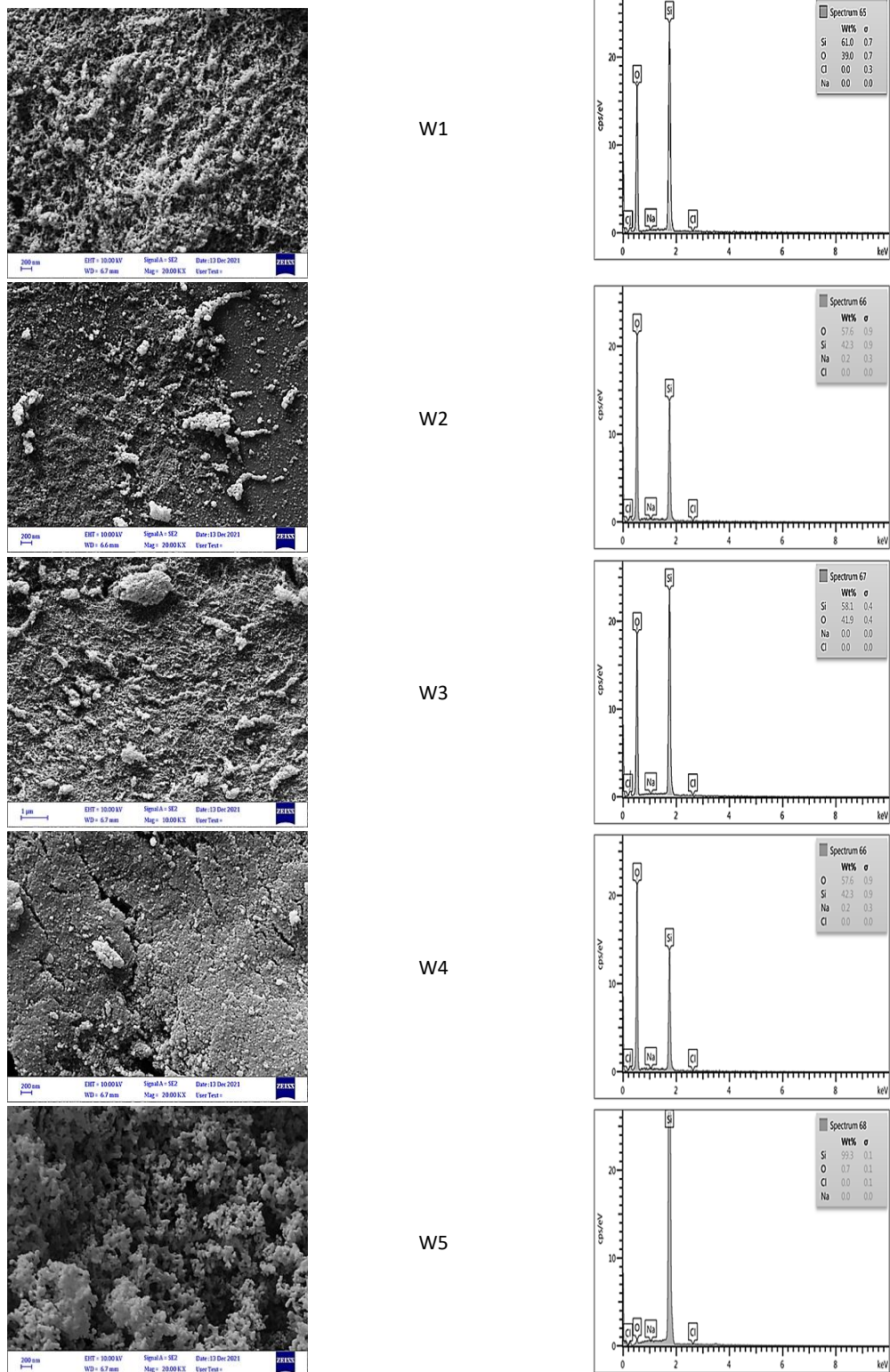
Figure 5. FESEM image for for W1, W2, W3, W4 and W5 samples

4. Conclusion

Numerous parameters influence silica aerogel properties. Precursors are crucial in the production of aerogel, and the low cost and safety are the primary reasons for using sodium silicate as a precursor in this work. The control of production procedures results in a superhydrophobic aerogel with a low surface area, microstructural integrity, low density, and low gel time. This leads to obtaining silica aerogel from sodium silicate with the best specifications at the lowest cost and time.

5. Acknowledgement

6. References

Aegerter, M. A., Leventis, N., & Koebel, M. M. (2011). Aerogels handbook: Springer Science & Business Media.

Al-Mothafer, Z., & Abdulmajeed, I. (2021). Comparative study in use sodium silicate instead of NH 4 OH as an alkaline basic catalyst to gelation unmodified silica aerogel based on tetraethoxysilane (TEOS). Journal of Ovonic Research, 17(4).

Al-Mothafer, Z., Abdulmajeed, I., & Al-Sharuee, I. (2021). effect of oxalic acid as a catalyst and dry control chemical additive (dcca) for hydrophilic aerogel base sodium silicate by ambient pressure drying. Journal of Ovonic Research Vol, 17(2), 175-183.

Al-sharuee, I. F. (2019). Thermal Conductivity Performance of Silica Aerogel after Exposition on Different Heating under Ambient Pressure. Baghdad Science Journal, 16(3 (Suppl.)), 0770-0770.

AL-Sharuee, I. F. (2021). Specifications study of Hydrophobic Silica Aerogel Doped with Rhodamine 6G Prepared via Sub-Critical Drying Technique. Iraqi Journal of Science, 483-489.

Al-sharuee, I. F., & Mohammed, F. H. (2019). Investigation study the ability of superhydrophobic silica to adsorb the Iraqi crude oil leaked in water. Paper presented at the IOP Conference Series: Materials Science and Engineering.

Bhagat, S. D., Kim, Y.-H., Suh, K.-H., Ahn, Y.-S., Yeo, J.-G., & Han, J.-H. (2008). Superhydrophobic silica aerogel powders with simultaneous surface modification, solvent exchange and sodium ion removal from hydrogels. Microporous Mesoporous Materials, 112(1-3), 504-509.

Bhagat, S. D., & Rao, A. V. (2006). Surface chemical modification of TEOS based silica aerogels synthesized by two step (acid–base) sol–gel process. Applied Surface Science, 252(12), 4289-4297.

Cheng, Y., Xia, M., Luo, F., Li, N., Guo, C., & Wei, C. s. (2016). Effect of surface modification on physical properties of silica aerogels derived from fly ash acid sludge. Colloids Surfaces A: Physicochemical Engineerin Aspects, 490, 200-206.

Daniel, C., Longo, S., Ricciardi, R., Reverchon, E., & Guerra, G. (2013). Monolithic nanoporous crystalline aerogels. Macromolecular rapid communications, 34(15), 1194-1207.

Dorcheh, A. S., & Abbasi, M. (2008). Silica aerogel; synthesis, properties and characterization. Journal of materials processing technology, 199(1-3), 10-26.

Durães, L., Ochoa, M., Rocha, N., Patrício, R., Duarte, N., Redondo, V., & Portugal, A. (2012). Effect of the drying conditions on the microstructure of silica based xerogels and aerogels. Journal of nanoscience nanotechnology, 12(8), 6828-6834.

Feng, Q., Chen, K., Ma, D., Lin, H., Liu, Z., Qin, S., . . . Aspects, E. (2018). Synthesis of high specific surface area silica aerogel from rice husk ash via ambient pressure drying. Colloids Surfaces A: Physicochemical Engineering spects, 539, 399-406.

He, S., & Chen, X. (2017). Flexible silica aerogel based on methyltrimethoxysilane with improved mechanical property. Journal of Non-Crystalline Solids, 463, 6-11.

He, S., Huang, Y., Chen, G., Feng, M., Dai, H., Yuan, B., & Chen, X. (2019). Effect of heat treatment on hydrophobic silica aerogel. Journal of Hazardous materials, 362, 294-302.

Huang, Y., He, S., Feng, M., Dai, H., Pan, Y., & Cheng, X. (2019). Organic solvent-saving preparation of water glass based aerogel granules under ambient pressure drying. Journal of Non-Crystalline Solids, 521, 119507.

Khedkar, M. V., Somvanshi, S. B., Humbe, A. V., & Jadhav, K. (2019). Surface modified sodium silicate based superhydrophobic silica aerogels prepared via ambient pressure drying process. Journal of Non-Crystalline Solids, 511, 140-146.

Li, M., Jiang, H., Xu, D., Hai, O., & Zheng, W. J. J. o. N.-C. S. (2016). Low density and hydrophobic silica aerogels dried under ambient pressure using a new co-precursor method. 452, 187-193.

Mazrouei-Sebdani, Z., Salimian, S., Khoddami, A., & Shams-Ghahfarokhi, F. (2019). Sodium silicate based aerogel for absorbing oil from water: the impact of surface energy on the oil/water separation. Materials Research Express, 6(8), 085059.

Monshi, A., Foroughi, M. R., & Monshi, M. R. (2012). Modified Scherrer equation to estimate more accurately nano-crystallite size using XRD. World J Nano Sci Eng, , 2: 154, 160.

Nguyen, B. N., Meador, M. A. B., Medoro, A., Arendt, V., Randall, J., McCorkle, L., & Shonkwiler, B. (2010). Elastic behavior of methyltrimethoxysilane based aerogels reinforced with tri-isocyanate. ACS Applied Materials Interface, 2(5), 1430-1443.

Pan, Y., He, S., Cheng, X., Li, Z., Li, C., Huang, Y., & Gong, L. (2017). A fast synthesis of silica aerogel powders-based on water glass via ambient drying. Journal of Sol-Gel Science Technology, 82(2), 594-601.

Sarawade, P. B., Kim, J.-K., Hilonga, A., & Kim, H. T. (2010). Production of low-density sodium silicate-based hydrophobic silica aerogel beads by a novel fast gelation process and ambient pressure drying process. Solid State Sciences, 12(5), 911-918.

Shao, Z., Luo, F., Cheng, X., & Zhang, Y. (2013). Superhydrophobic sodium silicate based silica aerogel prepared by ambient pressure drying. Materials Chemistry, 141(1), 570-575.

Shi, M., Tang, C., Yang, X., Zhou, J., Jia, F., Han, Y., & Li, Z. (2017). Superhydrophobic silica aerogels reinforced with polyacrylonitrile fibers for adsorbing oil from water and oil mixtures. RSC advances, 7(7), 4039-4045.

Shirtcliffe, N., McHale, G., Newton, M., & Perry, C. (2003). Intrinsically superhydrophobic organosilica sol– gel foams. Langmuir, 19(14), 5626-5631.

Wagh, P., Ingale, S., & Gupta, S. C. (2011). New technology for rapid processing and moulding of silica aerogel materials in prescribed shapes and sizes and their characterization. Journal of sol-gel science technology, 58(2), 481-489.

Wang, J., Zhang, Y., Wei, Y., & Zhang, X. (2015). Fast and one-pot synthesis of silica aerogels via a quasi-solvent-exchange-free ambient pressure drying process. Microporous Mesoporous Materials, 218, 192-198.

Wang, X.-D., Sun, D., Duan, Y.-Y., & Hu, Z.-J. (2013). Radiative characteristics of opacifier-loaded silica aerogel composites. Journal of non-crystalline solids, 375, 31-39.

Wingfield, C., Franzel, L., Bertino, M. F., & Leventis, N. (2011). Fabrication of functionally graded aerogels, cellular aerogels and anisotropic ceramics. Journal of Materials Chemistry, 21(32), 11737-11741.

Zhang, X., Chen, Z., Zhang, J., Ye, X., & Cui, S. (2021). Hydrophobic silica aerogels prepared by microwave irradiation. Chemical Physics Letters, 762, 138127.

Zhao, Y., Li, Y., & Zhang, R. (2018). Silica aerogels having high flexibility and hydrophobicity prepared by sol-gel method. Ceramics International, 44(17), 21262-21268.

Zhou, B., Shen, J., Wu, Y., Wu, G., & Ni, X. (2007). Hydrophobic silica aerogels derived from polyethoxydisiloxane and perfluoroalkylsilane. Materials Science Engineering: C, 27(5-8), 1291-1294.